The use of next generation Nitinol for medical implants

2

Alan R. PELTON, Sean M. PELTON, Jochen ULMER, Dave NIERDERMAIER,

Katarzyna PLASKONKA-WEISSENBURGER, Michael R. MITCHELL, Payman SAFFARI

This article reviews the use of Nitinol endovascular devices and the effects of biomechanics, design, and Nitinol microstrucutral purity on fracture.
Nitinol self-expanding stents are used to treat peripheral arterial disease, specifically in the superficial femoral artery (SFA) and popliteal artery (PA), and are prone to fracture with early generation stent designs and materials.
Nitinol self-expanding stents have become the standard of care for occlusive arterial disease following balloon angioplasty. Nitinol stents have been shown to improve the effectiveness of PAD treatment of the SFA/PA with a restenosis rate as low as 17.9% and patency rates of more than 85% at 18 months. Nevertheless, follow-up procedures show stent fracture rates up to 52% with some stent designs. This article will review the improvements in Nitinol stent technology due to:
1. Better understanding of the *in vivo* biomechanical deformation dynamics
2. Ingenuity in stent design
3. Improvements in the grades of "microclean" Nitinol
Newer stent designs used in the SFA show promise with improved patency rates and lower fracture rates. Incorporation of the latest generation of high-purity Nitinol is expected to result in even lower fracture rates due to significantly smaller inclusion sizes and therefore improved response.

Introduction

Nitinol, a nearly equiatomic nickel-titanium alloy known for its unique shape memory, superelastic response, and biocompatibility has proved particularly successful in biomedical applications during the past two decades. It is now common practice to employ Nitinol in endovascular stents, vena cava filters, transcatheter valve replacements, neurovascular occlusion devices, orthodontic files, orthopedic implants, and guidewires for minimally invasive procedures[1]. Both superelasticity and shape memory are driven by a stress- and/or temperature-induced martensitic phase transformations that allows recoverable accommodation of up to 8% strain[2]. With this magnitude of strain recovery, Nitinol enables minimally invasive procedures and thereby reduces unnecessary patient trauma[1].

Nitinol self-expanding stents have become the standard of care for occlusive arterial disease following balloon angioplasty[3]. Nitinol stents are manufactured in their open configuration, compressed into a much smaller delivery catheter (the superelastic effect), and then pushed out of the catheter where they expand against the vessel wall upon release and exposure to body temperature (the shape memory effect)[4].

Implantation of superelastic Nitinol stents after balloon angioplasty has demonstrated superior clinical outcomes for treatment of peripheral arterial disease (PAD), compared with conventional balloon angioplasty alone[5]. Nitinol stents have been shown to improve the effectiveness of PAD treatment of the superficial femoral artery (SFA)[6-9] with a restenosis rate as low as 17.9%[7] and patency rates of greater than 85% at 18 months[10]. In contrast, angioplasty had restenosis rates of 40-60% after one year[11] and stainless steel balloon-expandable stents had patency rates of 54% after one year[12].

Although the use of Nitinol for vascular implants has been quite successful, *in vivo* fractures and failures during follow-up procedures have been reported[6,13-19]. Jaff *et al.* pointed out that the SFA is at risk for PAD because it is an especially long vessel and is surrounded by two major flexion points[20]. Both hip and knee flexion act to shorten the SFA because the SFA is anterior in the upper part of the thigh and travels posterior in the lower part of the thigh. Furthermore, while most of the SFA resides in the adductor canal, some parts of the artery are not nearly constrained. These unconstrained sections can be subject to significant off-axis deflections, resulting from axial shortening, lack of SFA elasticity, and the localization of shortening. Jaff *et al.* illustrated the possible non-pulsatile forces exerted on the SFA that include torsion, compression, extension and flexion[20]. These deformations are well beyond the radial deformations typically considered for stent design as described by Stöckel, *et al.*[1] and those suggested by the 1995 version of the US FDA Stent Guidance Document for Intravascular Stents[21]. A number of reports based on clinical studies have begun to detail the impact of SFA fractures on restenosis rates. In the seminal SIROCCO trials, Nitinol self-expanding stents deployed in the SFA fractured in 12 out of 81 cases[6,7,9]. A subsequent study by Scheinert *et al.*[19] quantified the frequency of occurrence and clinical impact of Nitinol stent fractures for femoropopliteal stenting after a mean follow-up time of 10.7 months. Their investigation showed fracture rates of up to 37% with associated greater in-stent restenosis and reocclusion rates. It has been hypothesized that these stent fractures may be correlated to restenosis and the return of clinical symptoms[15,16,19].

To prevent vascular device failures, it is critical to understand the dynamic relationship of the implant with its vascular environment and then to use these boundary conditions in stent design with the most modern Nitinol material. Three major improvements have been made during the past several years to reduce the probability of Nitinol device fractures and will be reviewed in this article:

1. Focused research on understanding the biomechanical forces due to anatomical and physiological dynamic deformations.

2. Ingenuity in design of stents and other vascular implants.

3. Better understanding of the physics of Nitinol fatigue that has led to superior grades of "microclean" Nitinol.

Biomechanical deformations

Although *in vivo* biomechanical deformations work simultaneously (although at different frequencies and phase relationships), it is important to understand the individual contributions of deformations to dynamic motions. Recent literature has begun to clarify the anatomical and physiological environment of the SFA and associated popliteal arteries (PA) as discussed in the next section.

Musculoskeletal motions

Researchers at the FDA critically reviewed the femoropopliteal literature in order to understand the root cause for stent fractures[22]. Their literature review included a survey of 573 articles of which eight (plus three conference proceedings) met their criteria for inclusion in data comparison. They pointed out the difficulty of combining literature datasets due to differences in investigation design (for example, patient/subject selection, degree of deformation, stented/non-stented anatomies, imaging modality, and 2D *vs.* 3D imaging) as well as definitions of the SFA/PA region boundaries.

The authors first chose a set of definitions for the arterial boundaries and then grouped the data into three distinct regions: proximal/mid SFA (pSFA/mSFA), distal SFA/proximal PA (dSFA/pPA), and distal PA (dPA). Their summary of the pertinent findings according to arterial location and deformation are listed in Table I. In general, the dSFA/pPA and dPA regions present the greatest biomechanical deformations.

Table I: Summary of non-radial deformation averages and range data according to arterial location and in vivo motions (after [22])

Variable	pSFA/mSFA	dSFA/pPA	dPA	References
Axial Shortening, % Sitting/Stair Climbing	6.14 (0.4-29.5)	13.9 (1.5-26.0)	12.3 (3.5-18.5)	23-28
Axial Shortening, % Walking	4.0 (0-11)	8.1 (1.8-21.5)	7.7 (0-16.5)	23-28
Axial Twist, °/cm	2.1 (0.1-5.4)		3.5 (0.6-6.3)	27-29
Bending Radius of Curvature, mm	72.1 (19-206)		22.1 (13.0-33.8)	23-25,28,29
Local Compression (percent change in aspect ratio), %		4.6 (4.5-4.7)	12.5 (12.4-12.6)	30

Nitinol stent design

Scheinert *et al.* demonstrated that not all Nitinol stent designs have the same *in vivo* fracture rate; fractures occur in up to 50% of procedures with some stents and may induce clinically relevant restenosis[31]. Table II reproduced from their presentation is shown below.

These tabulated data indicate that stent design may be a major factor in the fracture rate and therefore the patency rate of these "first-generation" Nitinol stents placed in the femoral artery. Since these early results, it has become a high priority for stent manufacturers and the FDA to elucidate the *in vivo* mechanical environment and fracture mechanisms of implanted stents.

Bonsignore summarized the common features in "first-generation" Nitinol stents3 that include circumferential "strut V's" to provide radial support to the vessel and "bridges" to provide axial stiffness for loading and deployment. The exact geometry of these features is thought to be responsible for stent fractures during benchtop testing as well as the disparate results reported by Scheinert *et al.*[31]. The FDA recently approved several more flexible stents intended for use in the SFA/PA. These second generation stents feature "coil-spring" geometries to accommodate the axial motions during leg movements. We will briefly discuss two of these newer SFA stents below.

The BARD LifeStent® has a repeat section of circumferentially distributed struts following a helical pattern to produce a more flexible spring-like geometry[32]. During the RESILIENT clinical study the primary patency rates for the this stent were 81% at 6 months and 58% at 12 months[33]. It was observed that the fracture rates at 12 and 18 months were 3.1% and 4.2% although none of the patients with stent fractures lost primary patency or experienced a revascularization procedure[34,35].

Table II: Scheinert Data TCT-200 Obstructions Trial[31]

	Cordis SMART®	Bard Luminexx®	Abbott SelfX®
N (legs)	52	45	24
X-Ray Time	15.5 +/- 4.9	9.1+/-4.1	11+/-4
Patency (x-ray)	83%	59%	50%
Primary Patency at 12 Months	82%	27%	44%
% Stent Fractured	15%	52%	31%
Fracture not significant in patency	p = 0.7	p = 0.043	p=0.007

The Abbott SUPERA® peripheral stent is constructed from six pairs of closed-ended interwoven Nitinol wires that are arranged in a double-helical pattern designed to be both flexible and resistant to fracture[36]. Scheinert et al.[37] reported on the first retrospective study of the use of SUPERA stents in 107 atherosclerotic femoropopliteal lesions. The 6-, 12-, and 24-month cumulative primary patency rates were 93.1% ± 2.5%, 84.7% ± 3.6%, and 76.1% ± 4.5%, respectively. No stent fractures were observed on follow-up radiography[38]. Clinical results of patency and fracture rates from both of these recent stents represent a significant improvement over the first-generation stents listed in Table II.

Durability of Nitinol

This section will review Nitinol fatigue behavior, advances in computational analysis, and effects of Nitinol purity on fatigue fracture and durability.

Nitinol fatigue behavior

Figure 1 shows the fatigue behavior of Nitinol over a range of mean strains and strain amplitudes to illustrate the unusual response to these strains[39-41]. For the case of a Nitinol SFA stent, mean strains scale with the amount of oversizing of the stent diameter with respect to the vessel diameter. Strain amplitude corresponds to the pulse pressure or magnitude of the musculoskeletal motions[40]. In Figure 1, the blue circles and squares represent conditions where the laser-cut surrogate specimens survived 10M fatigue cycles. The

red circles and squares show conditions that fractured before 10M cycles; note that there are many fatigue conditions where some of the specimens survived and others fractured. Therefore, above the line, the probability of fracture is increasingly greater (*e.g.*, at greater strain amplitudes there are a greater number of red symbols). As such, from a design perspective it is important to ensure that the calculated fatigue strains for the medical device are below the line to obtain greater fatigue safety factors.
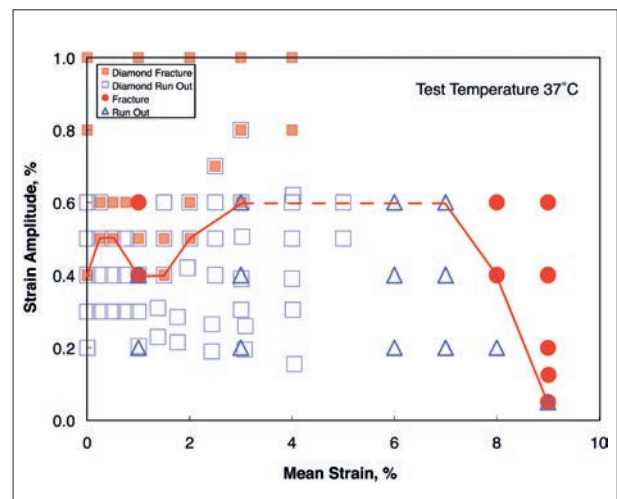
Figure 1: 10M-cycle constant-life diagram for (Generation I VAR) Nitinol, where the blue squares and triangles represent conditions where the laser-cut surrogate specimens survived 10M fatigue cycles. The red circles and squares show conditions that fractured before 10M cycles. Reprinted from Pelton[41] with permission from Springer.

Computational simulation of biomechanical motions

Figure 1 may be used to predict fracture or 10M-cycle survival of a medical device depending on the robustness of the computational analysis; translation of displacements into strains. As an example of such an investigation, we present the results of a finite element analysis (FEA) of a Nitinol Open Source Stent (OSS)[42] subjected to boundary conditions of 90°/90° knee/hip flexion from Nikanorov *et al.*[43]. The resultant mean strains and strain amplitudes for these simulated conditions are shown in Table III below.

Table III: Boundary conditions and fatigue strains for FEA simulation of the OSS[42]

Boundary Condition	Mean Strain %	Strain Amplitude %
8.6% Axial Compression	3.9	0.69
22.6mm Bending Radius	5.6	1.12

Figure 2a shows the resultant "point cloud" analysis of the 8.6% axial compression simulation of the OSS superimposed on the Nitinol fracture diagram from Figure 1; the color strain map of the OSS with the location of the maximum strain amplitude is also shown for these conditions[42]. The point cloud shows all of the combinations of mean strain and strain amplitudes from each of the 165,912 elements analyzed for the OSS. As shown in this figure, much of the stent has fatigue strains less than the 10M-cycle fatigue limit with a corresponding lower probability of stent fracture in these regions. However, there are also several sections of the stent that exceed the strain-limit line that predicts a greater probability of fracture. Figure 2b shows bench top fatigue data from a Nitinol stent with a similar geometry to the OSS that was tested with six different axial compression conditions to 10M cycles (ten-year equivalent[44]). These benchtop data demonstrate that the stent is able to survive 10M cycles at ≤ 8% axial compression. At conditions of ≥ 10% axial compression, however, the stent shows fractures as early as 10^3-10^4 cycles (corresponding to 10 to 100 hours of implant time). As such, the FEA of the OSS is in good agreement with the benchtop results.
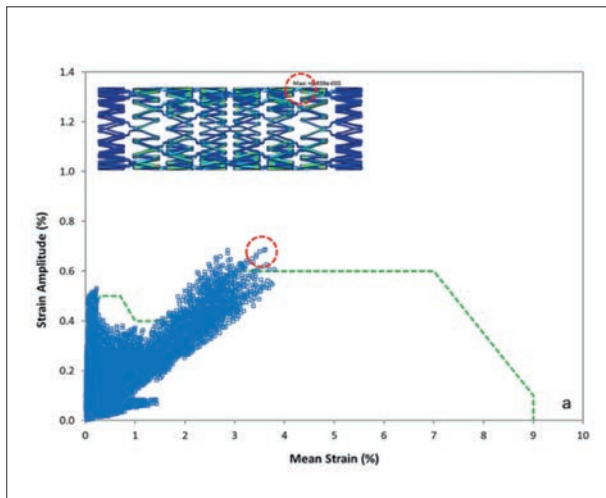
Figure 2: (a) FEA "point cloud" analysis of the mean strains and strain amplitudes from the 165,912 elements for the OSS device under 8.6% axial compression conditions. The inset image shows the location of the maximum strain amplitude of 0.69%[42].
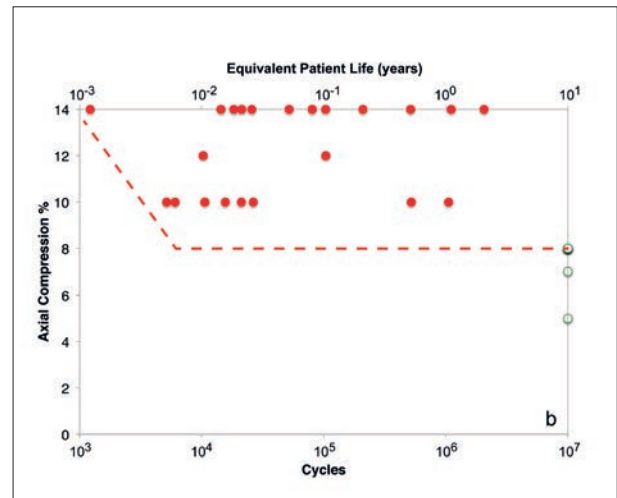
Figure 2: (b) Benchtop axial fatigue data from a Nitinol stent with similar geometry as the OSS. The red circles indicate stent fracture whereas the green open circles represent stent survival to 10M cycles. The data are consistent with the FEA simulations.

Figure 3 shows the point-cloud fatigue strain data from the computational simulation of the OSS under conditions of cyclic 22mm bend radius[42]. The FEA bend data from these severe dPA boundary conditions are superimposed on the Nitinol fatigue strain-limit diagram. These simulations result in a maximum strain amplitude of 1.12% with a mean strain of 5.6%; in this case, a much greater number of the stent elements exceed the fatigue strain limit. The greater probability of fracture with bend radii less than ~45mm is confirmed with the bench top data shown in Figure 3(b). The red circles indicate stent fracture whereas the green open circles represent stent survival to 10M cycles.

Effect of Nitinol "micro-purity" on device durability

During the past decade, manufacturers have accelerated the pace to provide "ultra-clean" Nitinol to the medical device industry. The key to these improvements is the reduction in oxide and carbide inclusion size and volume fraction[45-48]. A recent presentation summarized the evolution in commercially available Nitinol and is presented in Table IV.

The FDA overview article on SFA/PA biomechanics commented that the newer stents still fracture at a measurable rate although improvements have been made to make stents more durable, including finer surface finishes, increased flexibility, and longer lengths that reduce the need for overlapping[22]. However, the vast majority of commercially available Nitinol stents were manufactured from Generation I materials; therefore, the fatigue data presented in Figure 1 (Generation I VAR) represents the nominal behavior of the original SFA stents.
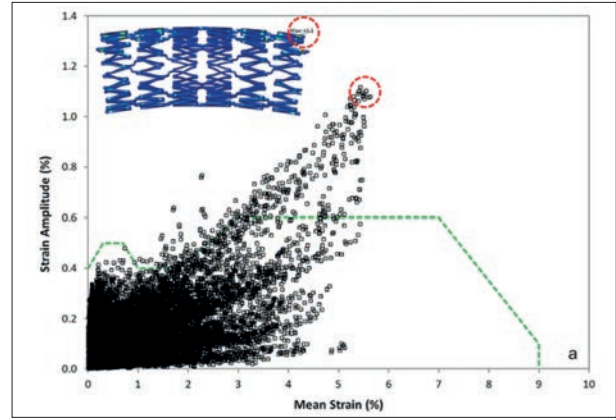
Figure 3: (a) FEA "point cloud" analysis of the mean strains and strain amplitudes from the 165,912 elements for the OSS device under cyclic 22mm bend radius conditions. The inset image shows the location of the maximum strain amplitude of 1.12% that corresponds to the greatest strain amplitude from the point cloud data (also circled)[42].
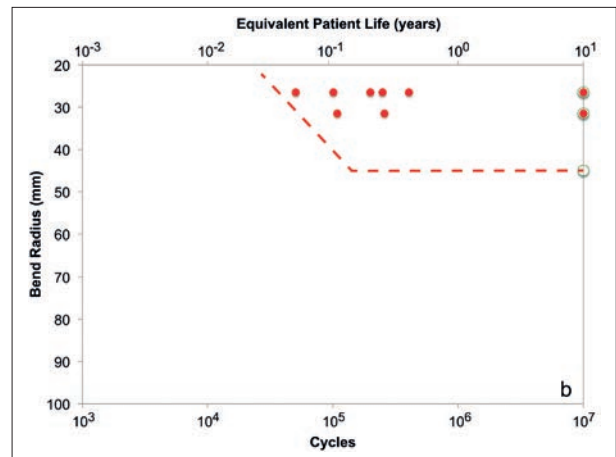
Figure 3: (b) Benchtop axial fatigue data from a Nitinol stent with similar geometry as the OSS that demonstrates that cyclic bend with bend radii less than ~45mm have a greater probability of fracture. The red circles indicate stent fracture whereas the green open circles represent stent survival to 10M cycles. The data are consistent with the FEA simulations in (a).

Table IV: Summary of Commercially Available Nitinol[48]

Material Classification	Year Introduced	Melt Source*	Conforms to ASTM F2063-12	Maximum Device Inclusion Size (μm)	Device Inclusion Area Fraction, %	Reference
Generation I	ca. 1990	VAR I	Yes	101	1.46	46
		VIM/VAR I		81	1.51	
Generation II	ca. 2005	VAR II	Yes	20	0.41	46,48
		VIM/VAR II	Yes	40	1.49	
		VIM II	Yes	50	2.67	
Generation III	ca. 2010	VAR/EBR III	Yes	<5	<0.5	48

*VAR = Vacuum Arc Remelt; VIM = Vacuum Induction Melt; EBR = Electron Beam Remelt

The recent advancement in Nitinol micro-cleanliness may also improve the durability of stents used in these challenging environments. For example, Robertson *et al.* recently reported on the improvements in bending fatigue with Generation II Nitinol[46]. Superelastic wires and diamond-shaped stent surrogates were tested from five different mill product suppliers with Generation I and II Nitinol, as summarized in Table IV.

These materials were processed for a transformation temperature of 20°C and were compared at 37°C with 6% crimp strain, 3% mean strain with a range of strain amplitudes to 10M fatigue cycles. Figure 4 shows the fatigue results from the diamond specimens in terms of statistical fracture probability, whereby the probability of fracture for each material is graphed as a function of strain amplitude. The Generation II VAR and VIM/VAR materials show a 2X improvement in the fatigue strain limit compared to the Generation I VAR and VIM/VAR Nitinol.
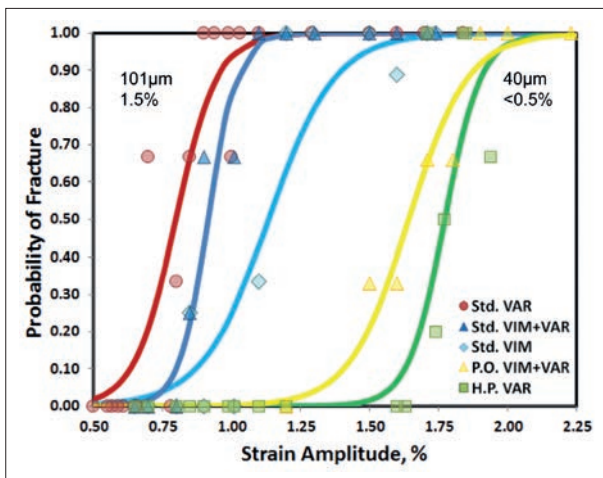
Figure 4: Probability of Nitinol diamond fracture at 10M cycles versus strain amplitude plots with a logit sigmoidal curve fit line for the five Generation I and II Nitinol materials. The maximum inclusion length (μm) and inclusion area fraction (%) for the VAR I and VAR II materials measured from the finished device are shown. Reprinted from Robertson, et al.[46] with permission from Elsevier.

This figure is quite revealing and demonstrates that **not all Nitinol material is the same with respect to fatigue properties.** A statistical analysis was done to determine the most probable factor to explain these results. Among the factors considered were stress concentrators (inclusion length and location, and grain size), probabilistic factors (area fraction of inclusions in %, density of inclusions/unit area), and macro-mechanics (transformation temperature, upper and lower plateau stress, strain amplitude, mean strain, test temperature). The model that most accurately represented the experimental data contained inclusion length, density of inclusions, and strain amplitude. Since strain amplitude is a test condition and not a material characteristic, the effects of inclusions are the most important factors. It was further shown that the inclusion length has a 4X influence over inclusion density to predict fatigue fracture. For example, in Figure 4 the material with the lowest fatigue strain limit (VAR I) has a device inclusion length of 101μm, whereas the material with the greatest strain limit (VAR II) has a reduced inclusion length of 40μm.

These comparative results afford great insight into the potential benefits of even greater purity micro-structures (*i.e.*, smaller inclusion size), such as those observed in Generation III Nitinol. This material is produced by electron beam remelting (EBR) of VAR material and is processed to obtain mechanical and transformational properties to meet the ASTM 2063-12 guidelines. A study was initiated to compare the fatigue response of Generation II and Generation III materials with diamond test coupons, similar to Robertson *et al.*[46]. The coupons were processed from 10mm OD x 0.53mm wall thickness Nitinol tubing to a transformation temperature of 20°C. Testing was done with VAR II, VIM/VAR II and VAR/EBR III at 37°C with a crimp strain of 6%, mean strain of 5%, and a range of strain amplitudes to 10M cycles (VAR/EBR III Nitinol was also tested with a 10% crimp strain). The results of these tests are shown in Figure 5a. As demonstrated in the 2015 study, the two Generation II materials have comparable fatigue behavior. However, VAR/EBR III shows a ~ 2X improvement in the fatigue strain limit over Generation II Nitinol. Figures 5b-d show representative microstructures of the three materials from the longitudinal direction from the coupons. The darker grey particles are oxide inclusions that form in the melt process; some of the particles in Figure 5c are carbides due to the melt practice in a graphite crucible. Table IV lists the maximum inclusion lengths and inclusion area fractions from the Generation II and III Nitinol materials.

The presentation of the fatigue data in Figures 4-5 in terms of fracture probability allows an estimation of fatigue strains that could have been operational for a given SFA stent. For example, Scheinert *et al.* reported fracture rates of 15%, 52%, and 31% for the Cordis SMART®, Bard Luminexx®, and Abbott SelfX® stents, respectively[31]. With reference to the Generation I VAR data in Figure 4, these fracture rates correspond to fatigue strain amplitudes of approximately 0.65%, 0.75%, and 0.70%, respectively. These strain amplitudes clearly exceed the fatigue strain limits shown in Figure 1 and are comparable to the 0.69% strain amplitude computed by Saffari for the OSS with 8.6%

axial compression[42]. If we consider the 1.12% strain amplitude due to dPA bending from Figure 3, we would expect fatigue fractures for the OSS with both Generation I materials as well as the VIM II Nitinol. However, from the results shown in Figure 5, if these OSS stents are instead manufactured from Generation II VAR, VIM/VAR or Generation III VAR/EBR, the probability of fracture would be significantly reduced. In fact, the fatigue safety factor for these conditions with VAR/EBR III Nitinol is 2.0%/1.12% > 1.7, confirming the low probability of fatigue fracture under these extreme *in vivo* conditions.

The decreased inclusion size and volume fraction produced by the EBR process, as illustrated in Figure 5, clearly leads to enhanced fatigue behavior compared with earlier Nitinol. This should be particularly true in the longer life regime to >100M cycles where inclusions govern fatigue response and a change in fracture initiation mode from surface to subsurface is dominant[49].
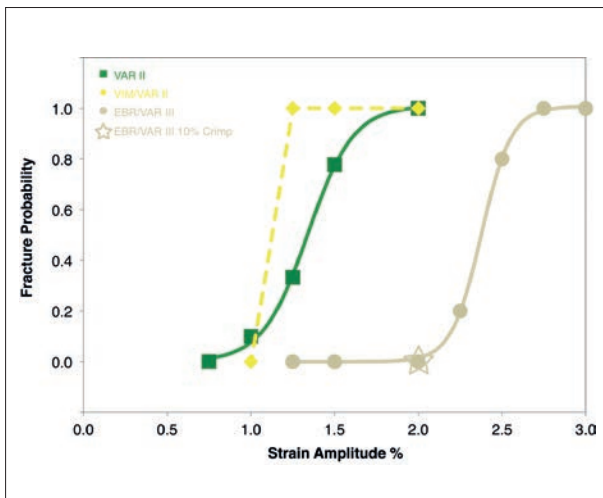
Figure 5: (a) Probability of Nitinol diamond fracture at 10M cycles versus strain amplitude plots for VIM/VAR II, VAR II, and EBR/VAR III Nitinol materials.

Conclusion

Although this article focused on SFA stents, it is expected that Generation II and especially Generation III Nitinol will be beneficial for use in even more challenging anatomies, such as aortic and mitral heart valve frames. The displacement strains in these environments are likely even greater than those in the femoral artery and may be the cause for reported aortic valve strut fractures[50].
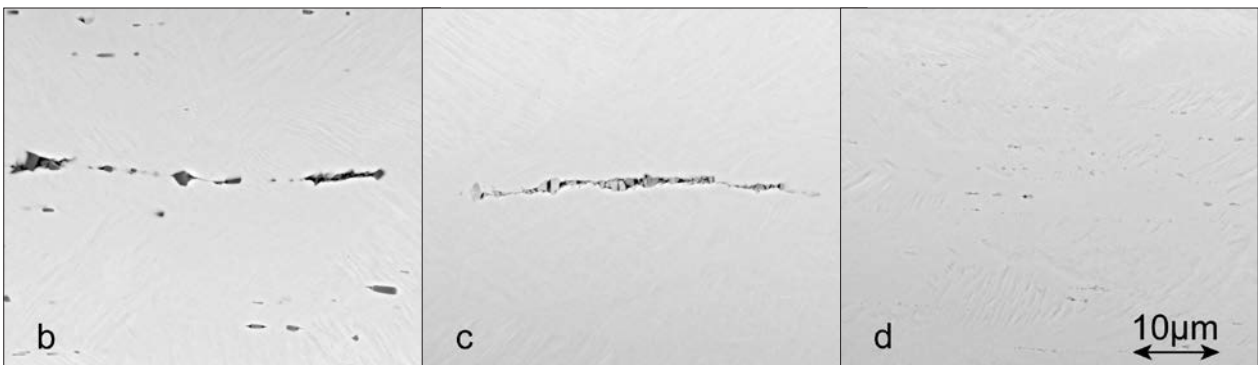
Figure 5: (b) VIM/VAR II microstructure showing a ~ 40μm long oxide inclusion "stringer"; (c) VAR II microstructure showing a ~ 40μm long oxide inclusion "stringer"; (d) VAR/EBR III microstructure showing ≤ 2μm oxide inclusions. After Pelton, et al. (2017).

References

1. Stöckel D, Pelton AR, Duerig T. Self-expanding Nitinol stents: Material and design considerations. *Eur Radiol* 2004; 14: 292-301.

2. Otsuka K, Ren X. Physical metallurgy of Ti–Ni-based shape memory alloys. *Progress in Materials Science* 2005; 50: 511-678.

3. Bonsignore, C. in *SMST* 2003: International Conference on Shape Memory and Superelastic Technologies (AR Pelton, TW Duerig eds) 2004: pp.519-28.

4. Duerig TW, Tolomeo DE, Wholey M. An overview of superelastic stent design. *Minim Invasive Ther Allied Technol* 2000; 9: 235-46.

5. Schillinger M, Sabeti S, Loewe C, Dick P, Amighi J, Mlekusch W, et al. Balloon angioplasty versus implantation of Nitinol stents in the superficial femoral artery. *N Engl J Med* 2006; 354: 1879-88.

6. Duda SH, Pusich B, Richter G, Landwehr P, Oliva VL, Tielbeek A, et al. Sirolimus-eluting stents for the treatment of obstructive superficial femoral artery disease: six-month results. *Circulation* 2002;106: 1505-9.

7. Duda SH, Bosiers M, Lammer J, Scheinert D, Zeller T, Tielbeek A, et al. Sirolimus-eluting versus bare Nitinol stent for obstructive superficial femoral artery disease: the SIROCCO II trial. *J Vasc Interv Radiol* 2005; 16: 331-8.

8. Sabeti S, Mlekusch W, Amighi J, Minar E, Schillinger M. Primary patency of long-segment self-expanding Nitinol stents in the femoro-popliteal arteries. *J Endovasc Ther* 2005; 12: 6-12.

9. Duda SH, Bosiers M, Lammer J, Scheinert D, Zeller T, Oliva V, et al. Drug-eluting and bare Nitinol stents for the treatment of athero-sclerotic lesions in the superficial femoral artery: Long-term results from the SIROCCO Trial. *J Endovasc Ther* 2006; 13: 701-10.

10. Henry M. Amor M, Beyar R, Henry I, Porte JM, Mentre B, et al. Clinical experience with a new Nitinol self-expanding stent in peripheral artery disease. *J Endovasc Surg* 1996; 3: 369-9.

11. Dormandy J, Rutherford B. Management of peripheral arterial disease. *J Vasc Surg* 2000; 31: S1-S296.

12. Gordon IL, Conroy RM, Arefi M, Tobis JM, Stemmer EA, Wilson SE. Three-year outcome of endovascular treatment of superficial femoral artery occlusion. *Arch Surg* 2001; 136: 221-228.

13. Allie D, Hebert C, Walker C. Nitinol stent fractures in the SFA. *Endovascular Today* 2004: 22-34.

14. Chang IS, Chee HK, Park SW, Yun IJ, Hwang JJ, Lee SA, et al. The primary patency and fracture rates of self- expandable Nitinol stents placed in the popliteal arteries, especially in the P2 and P3 segments, in Korean patients. *Korean J Radiol* 2011; 12: 203-9.

15. Vogel TR, Shindelman LE, Nackman GB, Graham AM. Efficacious use of Nitinol stents in the femoral and popliteal arteries. *J Vasc Surg* 2003; 38: 1178-83.

16. Haverizadeh BF, et al. Long-term outcome of superficial femoral artery stenting using self-expandable Nitinol stents compared to stainless steel stents: A retrospective study. *J Am Coll Cardiol* 2003; 41: 79-80.

17. Jacobs TS, Won J, Gravereaux EC, Faries PL, Morrissey N, Teodorescu VJ, et al. Mechanical failure of prosthetic human implants: a 10-year experience with aortic stent graft devices. *J Vasc Surg* 2003; 37: 16-26.

18. Rocha-Singh KJ, Scheer K, Rutherford J. Nitinol stent fractures in the superficial femoral: Incidence and clinical significance. *J Am Coll Cardiol* 2003; 79A: 868-864.

19. Scheinert D, Scheinert S, Sax J, Piorkowski C, Bräunlich S, Ulrich M, et al. Prevalence and clinical impact of stent fractures after femoropopliteal stenting. *J Am Coll Cardiol* 2005; 45: 312-5.

20. Jaff MR. The nature of SFA disease. *Endovascular Today* 2004: 3-5.

21. FDA. *Guidance Document for Intravascular Stents* 1995.

22. Ansari F, Pack LK, Brooks SS, Morrison TM. Design considerations for studies of the biomechanical environment of the femoropopliteal arteries. *J Vasc Surg* 2013; 58: 804-13.

23. Nikanorov A, Schillinger M, Zhao H, Minar E, Schwartz LB. Assessment of self-expanding Nitinol stent deformations implanted into the femoropopliteal artery. *Eurointervention* 2013; 9: 730-7.

24. Ganguly, A. et al. In-vivo imaging of femoral artery Nitinol stents for deformation analysis. *JVIR* 2011; 22: 244-249.

25. Smouse HB, Nikanorov A, LaFlash D, Smouse H, Nikanorov A, LaFlash D. Biomechanical forces in the femoropopliteal arterial segment. *Endovasc Today* 2005; (June): 60-6.

26. Nikanorov A, Smouse HB, Osman K, Bialas M, Shrivastava S, Schwartz LB. Fracture of self-expanding Nitinol stents stressed in vitro under simulated intravascular conditions. *J Vasc Surg* 2008; 48: 435-40.

27. Klein AJ, Chen SJ, Messenger JC, Hansgen AR, Plomondon ME, Carroll JD, et al. Quantitative assessment of the conformational change in the femoropopliteal artery with leg movement. *Catheter Cardiovasc Interv* 2009; 74: 787-98.

28. Cheng CP, Wilson NM, Hallett RL, Herfkens RJ, Taylor CA. In vivo MR angiographic quantification of axial and twisting deformations of the superficial femoral artery resulting from maximum hip and knee flexion. *J Vasc Interv Radiol* 2006; 17: 979-87.

29. Cheng CP, Choi G, Herfkens RJ, Taylor CA. The effect of aging on deformations of the superficial femoral artery resulting from hip and knee flexion: Potential clinical implications. *J Vasc Interv Radiol* 2010; 21: 195-202.

30. Brown R, Nguyen TD, Spincemaille P, Prince MR, Wang Y. In vivo quantification of femoral-popliteal compression during isometric thigh contraction: Assessment using MR angiography. *J Magn Reson Imaging* 2009; 29: 1116-24.

31. Scheinert D. TCT 2004, Washington, DC, USA. (oral communication)

32. (http://www.accessdata.fda.gov/cdrh_docs/pdf7/P070014b.pdf, 2009).

33. Published 3-year RESILIENT data support Bard's LifeStent in the SFA. *Endovascular Today* 2012.

34. Laird JR, Katzen BT, Scheinert D, Lammer J, Carpenter J, Buchbinder M, et al. Nitinol stent implantation vs. balloon angioplasty for lesions in the superficial femoral artery and proximal popliteal artery: twelve-month results from the RESILIENT randomized trial. *Circ Cardiovasc Interv* 2010; 3: 267-76.

35. Laird JR, Katzen BT, Scheinert D, Lammer J, Carpenter J, Buchbinder M, et al. Nitinol stent implantation vs. balloon angioplasty for lesions in the superficial femoral and proximal popliteal arteries of patients with claudication: Three-year follow-up from the RESILIENT randomized trial. *J Endovasc Ther* 2012; 19: 1-9.

36. Bishu K, Armstrong EJ. Supera self-expanding stents for endo-vascular treatment of femoropopliteal disease: a review of the clinical evidence. *Vasc Health Risk Manag* 2015; 11: 387-95.

37. Scheinert D, Grummt L, Piorkowski M, Sax J, Scheinert S, Ulrich M, et al. A novel self-expanding interwoven Nitinol stent for complex femoropopliteal lesions: 24-month results of the SUPERA SFA registry. *J Endovasc Ther* 2011; 18: 745-52.

38. Werner M, Paetzold A, Banning-Eichenseer U, Scheinert S, Piorkowski M, Ulrich M, et al. Treatment of complex atherosclerotic femoropopliteal artery disease with a self-expanding interwoven Nitinol stent: midterm results from the Leipzig SUPERA 500 registry. *Euro Intervention* 2014; 10: 861-8.

39. Tabanli RM, Simha NK, Berg BT. Mean stress effects on fatigue of NiTi. *Mater Sci Eng A* 1999; 644-8.

40. Pelton AR, Schroeder V, Mitchell MR, Gong XY, Barney M, Robertson SW. Fatigue and Durability of Nitinol Stents. *J Mech Behav Biomed Mater* 2008; 1: 153164.

41. Pelton AR. Nitinol fatigue: A review of microstructures and mechanisms. *JMEPEG* 2011; 20: 613-17.

42. Saffari P. in *SIMULIA Regional User Meeting* 2012 (Linz, Austria, 2012).

43. Nikanorov A, Schillinger M, Zhao H, Minar E, Schwartz L. B. in *SVS Vascular Annual Meeting*, Denver, CO, 2009.

44. Silva M. Average patient walking activity approaches two million cycles per year. *J Anthroplasty* 2002; 17: 693-7.

45. Robertson SW, Pelton AR, Ritchie RO. Mechanical fatigue and fracture of Nitinol. *International Materials Reviews* 2012; 57: 1-36.

46. Robertson SW, Launey M, Shelley O, Ong I, Vien L, Senthilnathan K, et al. A statistical approach to understand the role of inclusions on the fatigue resistance of superelastic Nitinol wire and tubing. *J Mech Behav Biomed Mater* 2015; 51: 119-31.

47. Urbano MF, Cadelli A, Sczerzenie F, Luccarelli, P, Beretta S, Coda, A. Inclusions size-based batigue life prediction model of NiTi alloy for biomedical applications. *Shape Memory and Superelasticity* 2015; 1: 240-251.

48. Pelton AR. et al. Diamond Fatigue Behavior of Generation II and III Nitinol. *SMST* (2017).

49. Bathias C. Fatigue limit in metals. Hoboken, NJ: John Wiley and Sons; 2014.

50. Chen M, Feng Y, Tang H, Xu Y, Wei X, Huang D. Strut fractures of CoreValve frames. *Int J Cardiol* 2013; 163: e42-3.